Springer

KSME

Journal of Mechanical Science and Technology 33 (5) (2019) 2075~2084
www.springerlink.com/content/1738-494x(Print)/1976-3824(Online)
DOI 10.1007/s12206-019-0411-1

Mechanism and force-energy parameters of a hollow shaft's multi-wedge synchrostep cross-wedge rolling †

Shuhua Zheng[1,2], Xuedao Shu[1,3,*], Sutao Han[1,3] and Penghui Yu[1,3]

[1]*Faculty of Mechanical Engineering and Mechanics, Ningbo University, Ningbo 315211, China*
[2]*School of Mechanical Engineering, Ningbo University of Technology, Ningbo 315016, China*
[3]*Part Rolling Key Laboratory of Zhejiang Province, Ningbo 315211, China*

(Manuscript Received April 25, 2018; Revised November 2, 2018; Accepted January 11, 2019)

Abstract

First, the rotation condition of a hollow shaft's multi-wedge synchrostep cross-wedge rolling (MSCWR) is determined and the relevant influencing rule is illustrated based on a mechanical model of the hollow shaft and the theory of solid shaft's rotation condition. The influence rule states that the increasing number of wedges increases the shrinkage rate of the hollow shaft and diminishes the rotation conditions, which can be improved by increasing μ on the forming surface of the hollow rolling mold, setting the stretching β, and forming α angles at approximately 4°-12° and 15°-35°, respectively. Second, a rigid-plastic finite element model is established for the hollow shaft with MSCWR by using the DEFORM-3D software, and the deformation mechanism of the hollow shaft is illustrated. The deformation degree of the rolling piece at the stretching stage decreases gradually from the surface to the interior of the hollow shaft, and radial compressive and transverse tensile strains interact with each other, thus resulting in an elliptic cross section of the hollow shaft. Stress field is mainly distributed in the exterior margin and then permeates into the inner part along the direction of the wall thickness, gradually transforming from compressive stress into tensile stress. Third, the influence of mechanical parameters on hollow shaft rolling is analyzed. The increased stretching angle increases the radial force, transverse force, and rolling torque and decreases the axial force. Moreover, the enlarged forming angle reduces the radial and transverse forces, while the decreased rolling torque increases the axial force. Finally, the 1:5 MSCWR experiment on the hollow shaft verifies the proposed finite element model's accuracy. Results of the research provide a theoretical basis for the MSCWR of a precise hollow shaft.

Keywords: Hollow shafts; MSCWR; Stress and strain; Force energy parameters

1. Introduction

Demand for railway axles is increasing in China owing to the rapid development of railway transportation, especially for high-speed railways. As the core component of high-speed train bogies, the hollow shaft is essential to the safe operation of high-speed trains. Foreign advanced high-speed trains, such as Germany's ICE, France's TGV, and Japan's new high-speed railway, have recognized the necessity of utilizing hollow shafts. The application of hollow shafts has remarkably reduced the weight of the wheel and the force between wheel and axle. This type of application is an effective solution to the lightweight railway. At present, most hollow shafts are forged by air hammer or rapid forging hydraulic press [1], which has limitations such as low material utilization, poor production environment, and heavy pollution. Cross-wedge rolling (CWR) is a new technology that has the advantages of high efficiency and material-saving capability [2, 3]. Multi-wedge synchrostep CWR (MSCWR) refers to the plastic deformation that utilizes multi-wedge molds to conduct radial compression and axial extension on the workpiece. This approach can significantly economize roller surface and improve rolling efficiency [4]. However, its actual application and promotion have been hindered by problems, such as complicated mold design, poorer rotation condition compared with that of solid shaft rolling, and difficulty in ensuring inner surface quality. Therefore, clarifying the mechanism and force energy parameters of a hollow shaft's MSCWR is necessary.

This study focuses on the solid long shafts of MSCWR technology in China. Shu [5, 6] conducted systematic studies on the force-energy parameters and forming mechanism of multi-wedge rolling. Zhao [7, 8] analyzed the influence of interface quality process parameters on multi-wedge rolling. Experts have conducted research on hollow shafts in CWR technology from different perspectives. Urankar [9, 10] established the fracture condition of the hollow shaft's CWR and developed a friction model of the shaft's critical rolling. Pater

*Corresponding author. Tel.: +86 13957878831, Fax.: +86 574 87600134
E-mail address: shuxuedao@nbu.edu.cn
† Recommended by Editor Chongdu Cho

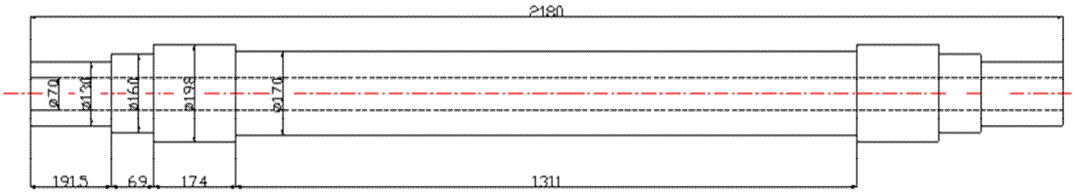

Fig. 1. Long hollow shaft model.

[11-13] studied the hollow shaft's stable rolling condition. Domestic researchers, such as Ding [14, 15], performed the thermo-mechanical coupling forming process of the hollow shaft with equal inner diameter using CWR. Ji [16] researched the formation and microstructure evolution of 21-4N for the hollow valve with CWR. Yang [17] studied the influence of flattening deformation on the formation of hollow parts in CWR. However, the cited studies are limited to single-wedge rolling. Few experts have studied the hollow shaft's MSCWR from a different viewpoint. Peng et al. [18] established how to control the ellipticity of the large and long thick-walled hollow shaft. Yu et al. [19] studied the effect of the process parameters on grain size of the hollow shaft made by MSCWR. Shu et al. [20] investigated the influence of mold technological parameters on the forming force parameters in multi-wedge rolling of railway hollow shafts. All these aforementioned studies provided a foundation for further promoting multi-wedge synchrostep rolling. However, hollow shaft rolling is a complex process that is difficult to implement in Chinese production.

This study first analyzes the rotation condition of the hollow shaft's MSCWR and establishes the rigid-plastic finite element model of the hollow shaft with a total length of 1311 mm in the DEFORM-3D software (Fig. 1). Then, it studies the deformation characteristics of the stretching stage in the course of rolling by applying multi-wedge synchrostep rolling technique. The law of stress-strain and energy parameters was obtained in the rolling process of the hollow shaft. Finally, experiments were conducted to validate the finite element model for presenting the mechanism and the force-energy parameters of the hollow shaft's MSCWR. The results provide a reliable theoretical basis for industrial application of the hollow shaft's MSCWR.

2. Rotation condition of hollow shaft rolling by MSCWR

The rotation condition represents the premise of the hollow shaft's MSCWR. Fig. 2 shows the mechanical models of the solid and hollow shafts. Radial stiffness of the hollow shaft is poorer than that of the solid shaft, that is, The deformation and contact area of the hollow shaft will also increase when the rolling area increases. The contact area transforms into arc AC [Fig. 1(b)] from arc AB [Fig. 1(a)], and the angle θ corresponding to arc BC is increased. The rotation condition of the solid shaft's MSCWR [14] shows that dp_1, dp_2, dp_3… represent the distance between the two tangential frictional friction

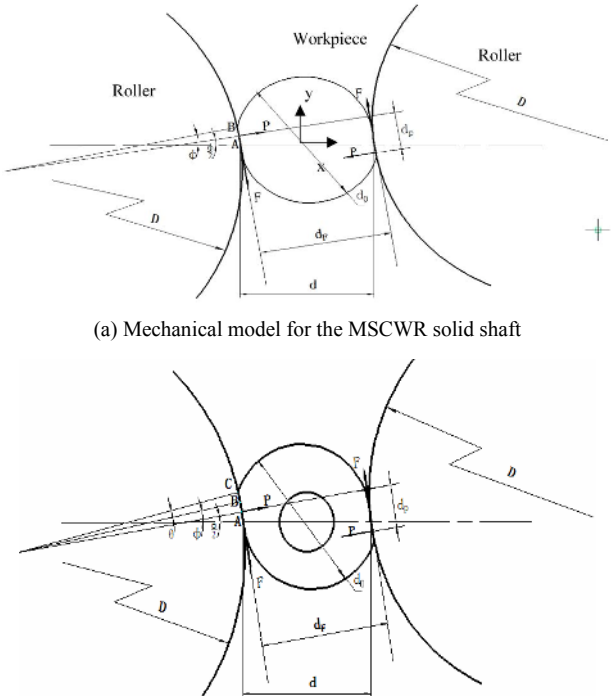

(a) Mechanical model for the MSCWR solid shaft

(b) Mechanical model for the MSCWR hollow shaft

Fig. 2. Mechanical model for the hollow and solid shafts.

forces F for each wedge. Similar to dp, d_{F1}, d_{F2}, d_{F3} … represent the distance between two normal forces P for each wedge. If the parameters of each wedge are the same, then $dp_1 = dp_2 = dp_3 = \ldots$, $d_{F1} = d_{F2} = d_{F3} = \ldots$ and $P_1 = P_2 = P_3 = d$, which is similar to the conditions of the hollow shaft's rotation. Therefore, when the hollow shaft is rotating, the critical friction coefficient μ between the wedge and workpiece should satisfy the following formula:

$$\mu \geq \frac{d_P}{d_F}. \tag{1}$$

For a hollow workpiece, the increase in deformation magnitude can be characterized by the angle θ. Fig. 2(b) shows that φ refers to the circular angle of the contact area, d is the diameter of the workpiece, and d_F is the distance between the two tangential friction forces, which is presented as

$$d_F = d\cos(\frac{\varphi+\theta}{2}). \tag{2}$$

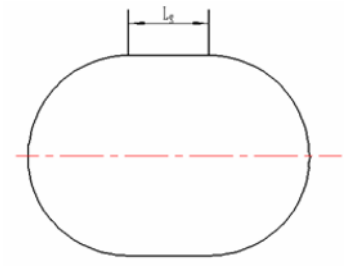

(a) Deformation of solid workpiece under compression

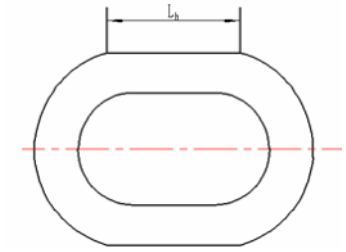

(b) Deformation of hollow workpiece under compression

Fig. 3. Deformation of solid and hollow shafts under compression.

d_p is the distance between the two positive pressure forces and is presented as

$$d_p = (D+d)\sin(\frac{\varphi+\theta}{2}) \tag{3}$$

where D represents the diameter of the roller. Eq. (4) can be inferred from the combination of Eqs. (1)-(3).

$$\mu \geq (1+\frac{D}{d})\tan(\frac{\varphi+\theta}{2}). \tag{4}$$

Fig. 3 shows the deformation of solid and hollow shafts under compression.

Ls refers to the contact length of the solid workpiece, arc AB, which is defined as

$$L_{AB} = L_S = \frac{D}{2}\varphi. \tag{5}$$

L_h refers to the contact length of the hollow workpiece, arc AC, which is defined as

$$L_{AC} = L_h = \frac{D}{2}(\varphi+\theta). \tag{6}$$

Given that m is the ellipticity parameter,

$$m = \frac{L_h}{L_s} = \frac{L_{AC}}{L_{AB}} = 1+\frac{\theta}{\varphi}. \tag{7}$$

It can be deduced from Eq. (7) that

$$\theta = (\mathrm{m}-1)\varphi. \tag{8}$$

Substituting Eq. (8) into Eq. (4),

$$\mu \geq (1+\frac{D}{d})\tan(\frac{m\varphi}{2}). \tag{9}$$

As $\frac{\varphi}{2}$ is extremely small, thus

$$\tan(\frac{m\varphi}{2}) \approx \mathrm{m}\tan(\frac{\varphi}{2}). \tag{10}$$

Fig. 2 shows that

$$\tan(\frac{\varphi}{2}) = \sqrt{\frac{dZ+Z^2}{D(\mathrm{D}+d)}} \tag{11}$$

where Z denotes the decrement of the multi-wedge finishing stage, which is presented as

$$\mathrm{Z} = \frac{d_0-d_1}{2} = \frac{1}{2}nk\pi d_k \tan\alpha\tan\beta. \tag{12}$$

In Eqs. (5)-(12), n is the number of wedges; k refers to the instantaneous stretching coefficient of the workpiece ($0 < k < 1$); d_k is the rolling diameter, $d_k = d_1+0.62(d_0-d)$; d_0 is the diameter of the workpiece; α is the forming angle; and β is the stretching angle. Substituting Eqs. (10) and (11) into Eq. (9) results in the following:

$$\mu^2 \geq m^2(1+\frac{d}{D})[\frac{Z}{d}+(\frac{Z}{d})^2] \tag{13}$$

where $\frac{Z}{d}$ refers to the relative compression. This value is small, and the value of $(\frac{Z}{d})^2$ is even smaller, indicating that it can be ignored. Hence, Eq. (13) can be simplified as

$$\mu^2 \geq m^2(1+\frac{d}{D})\frac{Z}{d}. \tag{14}$$

Substituting Eq. (12) into Eq. (14) can obtain the rotational condition of MSCWR via the following equation:

$$\tan\alpha\tan\beta \leq \frac{2d\mu^2}{nk\pi d_k m^2(1+\frac{d}{D})}. \tag{15}$$

Eq. (15) shows that the rotation conditions of the hollow shaft are influenced by the following factors. (1) The increased number of wedges worsens the rotation conditions. (2)

Table 1. Process parameters for simulation in every wedge.

Stretching angle β (°)			Forming angle α (°)			Section shrinkage (%)			Deflection angle θ_1 (°)	Deflection angle θ_2 (°)
1 wedge	2 wedges	3 wedges	1wedge	2 wedges	3 wedges	1 wedge	2 wedges	3 wedges	2 wedges	3 wedges
5°	6.5°	6.5°	45°		45°	22°		29°/56°	1°	2°

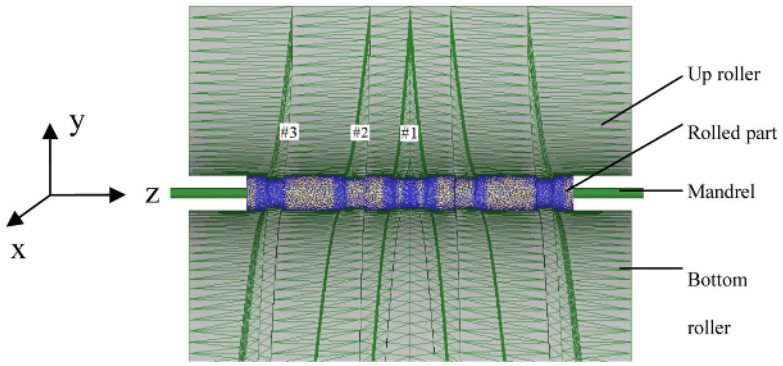

Fig. 4. FEM model of multi-wedge rolling hollow shafts.

The friction coefficient μ^2 has a significant effect on the rotation condition, which can be improved by increasing the μ on the forming surface of the hollow rolling mold. (3) When a high shrinkage rate of the hollow shaft exists, rotation worsens. (4) A small stretching angle β is favorable for rotation, but the decreased β will increase the stretch length; therefore, β should be set to 4°-12°. (5) A small α is favorable for rotation. However, the forming angle cannot be too small because it will result in the elliptical tendency of the workpiece, thereby hindering rotation. Generally, α is set to 30°-48°.

3. Finite element model of the hollow shaft's MSCWR

This study uses DEFORM-3D software to investigate the rule of internal stress and strain. The finite element modeling process and basic assumptions are obtained from our previous research [4]. The parameters selected in accordance with Eq. (13) are shown in Table 1, and Fig. 4 displays the finite element model. The billet, temperature, roller diameter, external diameter, and internal diameter are 42CrMo, 1100 °C, 630 mm, 202 mm and 60 mm, respectively. The author applies the established mathematical model of dynamic recrystallization of the material based on rigid-plastic finite element modeling. Mechanical properties of the material are as follows: E (roller's elasticity modulus) = 210 GPa, v (Poisson's ratio) = 0.3, density = 7.82×10^3 Kg/m^3, μ refers to the shear friction coefficient. The shear friction coefficient μ between the mold and rolled piece is a constant, which is typically μ = 2.

4. Deformation mechanism of the hollow shaft

4.1 Deformation characteristics

Fig. 5 shows the process of the hollow shaft's multi-wedge rolling. The process can be divided into eight typical phases: (1) Wedging stage of wedges #1, #2 and #3; (2) stretching stage of wedge #1; (3) stretching stage of wedge #2; (4) stretching stage of wedge #3; (5) stretching stage of wedges #1, #2 and #3; (6) rolling convergence stage of wedge #1 ; (7) finishing stage of wedge #2; (8) the end. Fig. 5 shows that the rolled piece gradually elongates along the axis with the decreased diameter in the course of MSCWR. The stretching stage is regarded as the major phase of the rolling process because radial compression and axial extension mainly occur in this phase. Therefore, stress and strain in the stretching stage are mainly analyzed in this section.

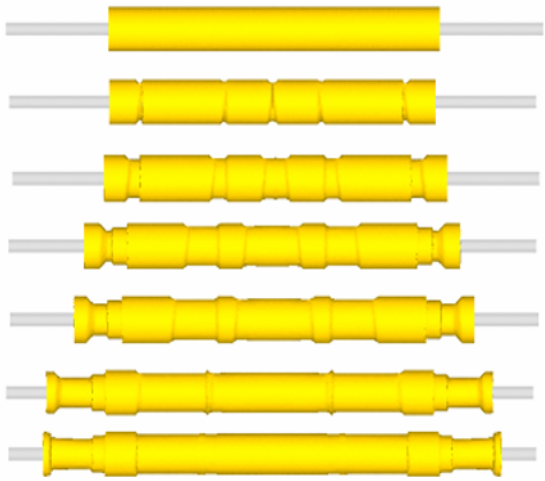

Fig. 5. Forming process of multi-wedge rolling hollow shafts.

4.2 Characteristics of strain field in the stretching stage

Fig. 6 displays the strain distribution on the longitudinal section of the workpiece's three-wedge stretching stage. The hollow workpiece is mainly characterized by radial compres-

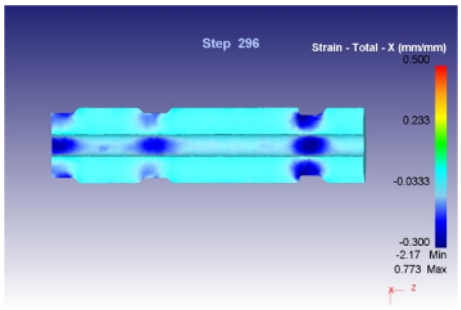

(a) Transverse strain ε_x

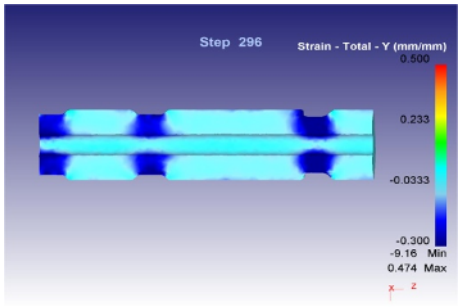

(b) Radial strain ε_y

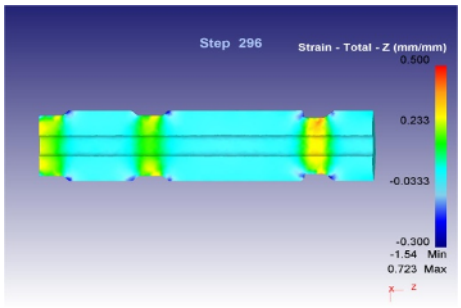

(c) Axial strain ε_z

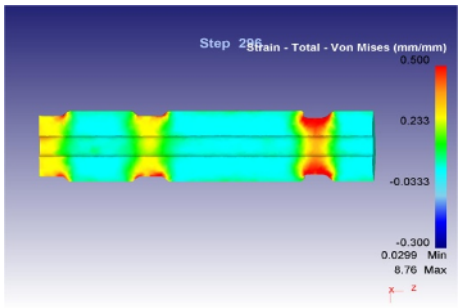

(d) Equivalent strain $\bar{\varepsilon}$

Fig. 6. Strain distribution of the longitudinal section for the stretching stage.

sion and axial extension deformation, and its inner hole is approximately round under the influence of the mandrel. Fig. 6(a) shows the distribution of transverse strain ε_x on the longitudinal section. Compressive strain occurs in the three-wedge rolling area for radial and transverse strains, which are more likely to occur in hollow shaft rolling than in solid shaft rolling. The mutual influence of both strains also leads to ovality

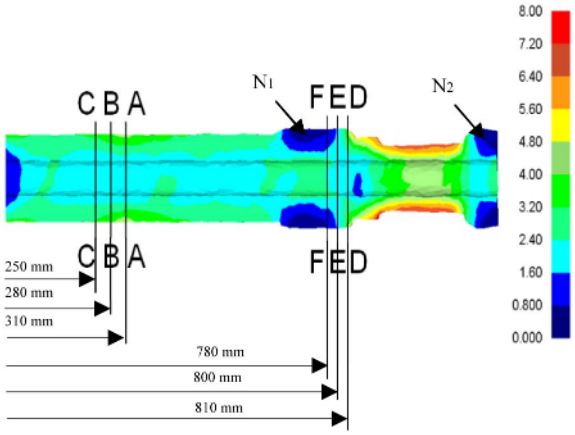

(a) Equivalent strain in the longitudinal section

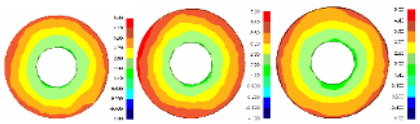

(b) Three sections of wedges 1 and 2 junctions

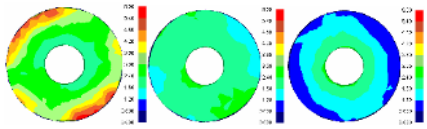

(c) Three sections of the shoulder

Fig. 7. Distribution of equivalent strain in the stretching stage.

in the cross section. Fig. 6(b) shows the distribution of longitudinal strain ε_y on the longitudinal section. Moreover, the maximum tensile strain occurs in the third wedge area with the maximum shrinkage rate. Strain also decreases gradually with the distance to areas where the wedge had effects, such that increased distance reduces strain. Fig. 6(c) refers to the distribution of axial strain ε_z on the longitudinal section, wherein its axial strain is the tensile strain in uniform distribution. In the section where the workpiece is in contact with the forming surface of the mold, a local small compression strain occurs due to the obstruction of metal flow. Fig. 6(d) presents the distribution of equivalent strain ε on the longitudinal section, wherein the deformation degree of the rolled three wedges gradually decreases from the surface to the interior. No strain occurs on the metal in the undeformed area of the workpiece during the entire process. Influenced by the mandrel, circumferential strain of the inner hole surface becomes uniform with the small strain value, and the rolled inner hole has the advantage of ellipticity.

The equivalent strain indicates the intensity of deformation and varies at different areas. Fig. 7 shows the longitudinal section of the hollow shaft, where the distribution of equivalent strain occurs in the typical section of the stretching stage after rolling. Fig. 7(a) presents that the most intensive deformation can be found at the right step with the equivalent strain

reaching 5.6-8.0 as the minimum equivalent strain occurs at N1 and N2. Fig. 7(b) shows the equivalent strain value of the typical sections A, B and C of the hollow axis that has an equal inner diameter. After studying all the typical circular-shaped sections, it can be inferred that the decreased distance from the center reduces deformation, and the equivalent strain in the center is only approximately 0.8 - 1.4. As for the B-B circular-shaped section, the equivalent strain on the surface is the maximum. Fig. 7(c) displays the equivalent strain of the typical sections D, E and F, where the D-D section has the maximum intensity of deformation with the equivalent strain reaching approximately 5.4-6.0 and the F-F section has the minimum deformation. The E-E section has medium intensity of deformation with the equivalent strain reaching approximately 1.6-2.4.

4.3 Feature of stress field in the stretching stage

Fig. 8 displays the stress field distribution on the longitudinal section of the three-wedge section. Transverse σ_x, longitudinal σ_y, and axial σ_z stresses found in the contact area between the workpiece and the mold's three wedges can all be classified as compressive stress. The maximum equivalent stress reaches up to 341 Mpa and gradually reduces from the surface to the center or even transforms into tensile stress. However, the metal of the rolling piece is compressed in the radial direction in the course of rolling and its inner wall and mandrel begin to extrude, resulting in the occurrence of stress. Fig. 8(a) shows the distribution of transverse stress σ_x, wherein the maximum compressive stress (353 Mpa) occurs at the contact area between the wedge and the mold. The surface metal flows during stretching, which leads to the flow of the inner metal. Consequently, stress gradually decreases in the direction of wall thickness until tensile stress is produced. Fig. 8(b) presents the distribution of longitudinal stress σ_y, which decreases from the contact surface between the workpiece and mold to the inner wall of the rolling piece. Fig. 8(c) shows the distribution of axial stress σ_z, which indicates that a rapid flow of metal occurs in the axial direction when it comes to the stretching stage. Hence, the value of axial stress in this stage is smaller than that of the wedging stage. Local compressive stress may also occur under the effect of wedge. Furthermore, the distribution of equivalent stress $\bar{\sigma}$ in Fig. 8(d) shows that the stress field is mainly distributed in the exterior margin and then permeates into the inner part with the stress in the direction of wall thickness gradually transforming into tensile stress. The forming rate is accelerated during the stretching stage because of the reduced resistance on the axial metal flow, and tensile strain is produced inside.

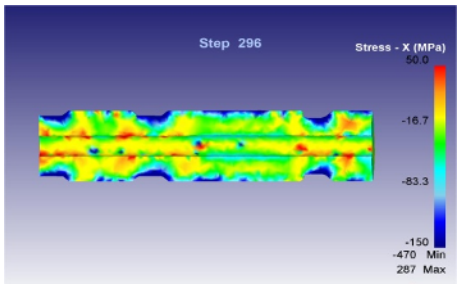

(a) Transverse stress σ_x

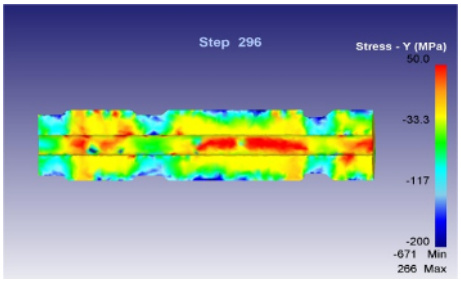

(b) Radial stress σ_y

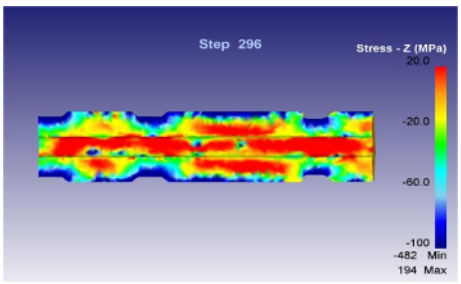

(c) Axial stress σ_z

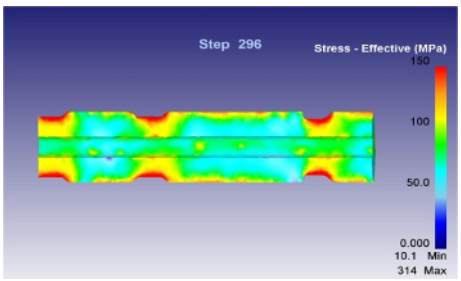

(d) Equivalent stress $\bar{\sigma}$

Fig. 8. Stress distribution in the longitudinal section for the stretching stage.

5. Influence of process parameters on the force-energy parameters of multi-wedge rolling

5.1 Effects of stretching angle

In the process of multi-wedge rolling, the stretching angle of the side wedge is typically limited by the main wedge. Thus, the author merely discusses the stretching angle of the main wedge when studying the stretching angle's effects on force-energy parameters. Fig. 9 shows that the author conducted experiments with various applied angles, such as β_1 (5°), β_2 (5.5°) and β_3 (6°).

Fig. 9 shows that force and torque parameters increase remarkably in the wedging stage and reach the maximum value at the end of this stage. Force energy parameters are relatively stable at the stretching phase as well. Along with the enlarging stretching angle, the radial and tangential forces are strength-

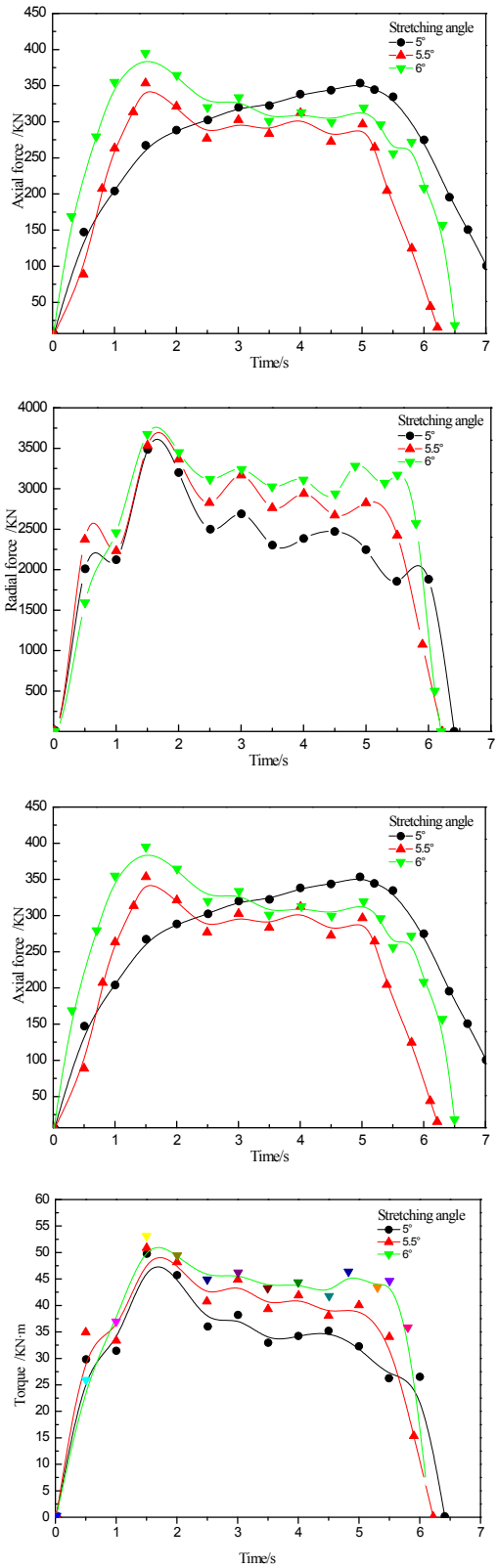

Fig. 9. Law of force-energy parameter under different stretching angles.

ened, axial force is diminished, and rolling torque is increased. Based on the formula $S = \pi r_k tg\beta$ (where S represents the axially compressed metal volume, r_k refers to the rolling radius of the workpiece, and β is the stretching angle), S and β are in direct ratio. Specifically, when the stretching angle is enlarged, metal flow in the deformation area will increase, and axial compression, deformation degree, and resistance to axial extension will also increase, leading to the worsened stress state and reduced axial tensile stress. Furthermore, the increased stretching angle increases the contact area where plastic deformation occurs in the radial direction. Therefore, it can be safely assumed that intensity of the radial force, tangential force, and rolling torque is directly proportional to the stretching angle. If the stretching angle is enlarged, then the contact area where plastic deformation occurs in the axial direction will decrease, the metal's axial flow trend will weaken, the contact area where the plastic deformation occurs in the radial direction will expand, and friction in the opposite flow direction of the metal flow will increase, thus producing a decreased axial force. Hence, it can be assumed that the axial force and stretching angle are in inverse ratio.

5.2 Effect of forming angle

The multi-wedge mold is taken as the research subject in this study. Parameters are set as follows: Forming angles of the main wedge are 35°, 40° and 45°; forming angle of the side wedge is 45°, external diameter of the semi-finished workpiece is 202 mm, and inner diameter is 60 mm. Fig. 10 shows the change of force-energy parameters under different forming angles of the main wedge.

The figure presents that a remarkable increase occurs in the force-energy parameters in the wedging stage, the maximum value is obtained at the end of the stage, and the parameters remain relatively steady in the stretching stage regardless of the occurrence of slight volatility. Radial and transverse forces relatively decrease along with the increasing forming angle as axial force increases. The enlarged forming angle increases the volume of axial flow of the metal in the rolling area and decreases the volume of radial flow, axial extension resistance to metal, and rolling force required by the plastic flow of metal. Meanwhile, the contact area between the part that undergoes plastic deformation and the roller is diminished along the radial direction. Furthermore, the combined effects of the two weaken the radial and transverse forces. The axial component of the positive pressure on the contact surface increases with the increased forming angle of the axial force along with the flow of metal in the axial direction, thereby leading to the increased axial force.

6. Experimental validations

Limited by the condition of the experimental mill, the hollow shaft is formed at the reduced scale size of 1:5. The experimental parameters are listed in Table 2. When the long shaft parts undergo MSCWR, the total length of the middle equivalent diameter shaft segment is 1311 mm (Fig. 1), which is mainly formed by the main (#1 in Fig. 11) and side (#2 in

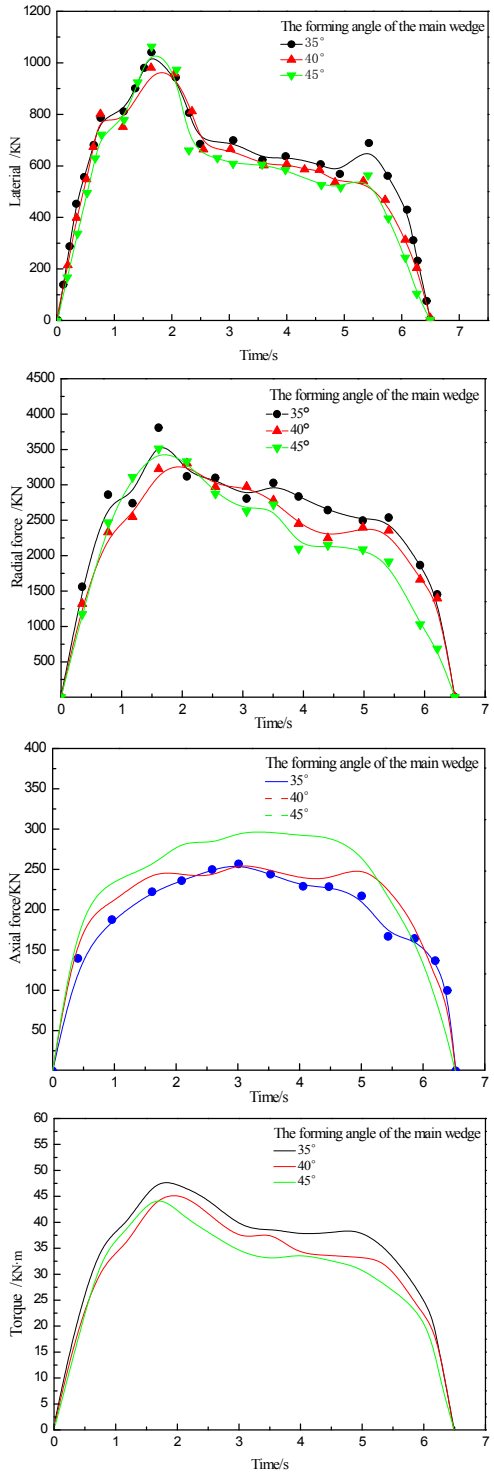

Fig. 10. Law of force-energy parameter under different main forming angles.

Fig. 11) wedges synchronously, and the rolling wedges are consistent with the finite element model (Fig. 4). After rolling the billet part, two gradient steps are formed at the transitional position between the main #1 and side #2 wedges. In this experiment, making the transitional shaft segment smooth is difficult, and further research must be conducted on achieving this step to optimize the mold in the future. Fig. 11 shows the experimental mold of the hollow shaft, and Fig. 12 presents the rolled experimental hollow shaft.

Table 2. Process parameters of MCR hollow shafts.

Parameters	Value	Parameters	Value
Hollow shaft outer diameter/(mm)	40	Roller speed/(r/min)	8
Hollow shaft inner diameter/(mm)	12	Roller diameter/(mm)	620
Hollow shaft length/(mm)	330	Rolling temperature/(°C)	1100
Mandrel diameter/(mm)	11.5	Wedge quantities of the roller	3

Fig. 11. 1:5 hollow railway shaft rolling mold.

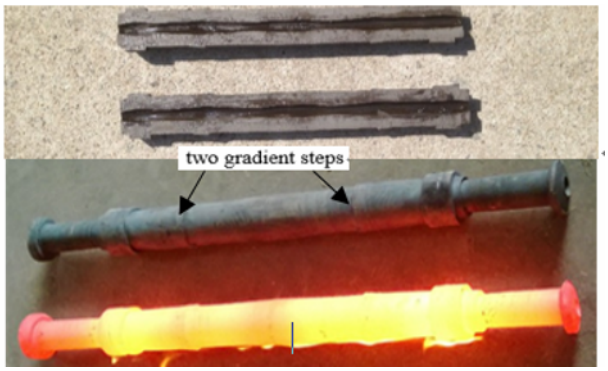

Fig. 12. 1:5 hollow railway shafts after the experiment.

To measure these force-energy parameters and verify the accuracy of the aforementioned calculation mode, the sensor node, battery, and strain gauge are fixed on the rotation axis. In addition, the strain value of the rotation axis is measured directly by the experimenter, and then the strain torque is obtained to calculate the torque value using the corresponding software. The measuring equipment of rolling torque in the experiment is shown in Fig. 13(a), while Fig. 13(b) shows the torque results from FEM, where M and T refer to the simulated and experimental data, respectively. The maximum rolling torque is 14.3 KN·m, where the number measured by the finite element method reaches up to 14.96 KN·m. An average deviation of 7 % is obtained between the test and simulation results, which, at less than 10 %, is proof of the credibility of

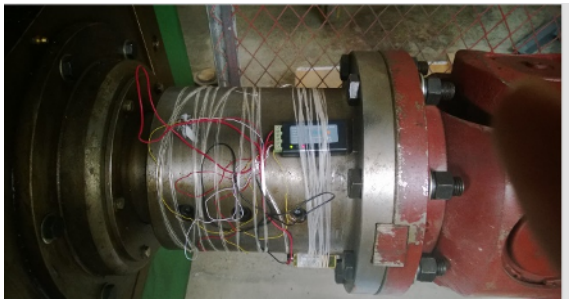

(a) Placement of the strain gauge

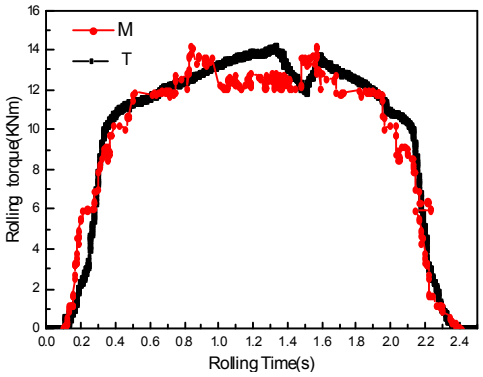

(b) Torque results from FEM and the experiment

Fig. 13. Torque of MCR in the experiment.

the analysis.

7. Conclusions

The rotation conditions of the hollow shaft's multi-wedge rolling are determined based on the mechanical model of hollow shaft rolling. These conditions provide a theoretical guide for designing the parameters of the mold for the hollow shaft's MSCWR. The study on the mechanism of the hollow shaft's MSCWR reveals that the deformation degree of the rolling piece at the stretching stage decreases gradually from the surface to the interior of the hollow shaft. Moreover, radial compressive and transverse tensile strains are likely to occur in the hollow shaft. The two strains may interact with each other, resulting in the elliptic cross section of the hollow shaft. Meanwhile, tensile strain is observed during the three-wedge rolling process, and the maximum tensile strain appears in the third wedge.

Furthermore, this study analyzes the force-energy parameters of high-speed hollow railway shafts produced by MSCWR. Research shows that the increased stretching angle increases the radial force, transverse force, and rolling torque but decreases the axial force. The increased forming angle also reduces the radial and transverse forces, and the decreased rolling torque increases the axial force.

The experimental results verify the finite element model of MSCWR and provide a theoretical foundation for the implementation of multi-cross wedge rolling technology.

Acknowledgements

This study was supported by the National Natural Science Foundation of China (No. 51475247), the Scientific and Technology Plan Research Projects of Zhejiang Province Projects Department (No. 2016C31018), and the Natural Science Foundation of Ningbo (No. 2017 A610087).

References

[1] C. M. Li, X. D. Shu and Z. H. Hu, The research and the actuality on methods of forming railway shaft, *Metallurgical Equipment*, 6 (2006) 5-8.

[2] X. D. Shu et al., *Cross Wedge Rolling Theory and Forming Technology*, Beijing: Science Press (2014) 1-10.

[3] J. C. Liang et al., Influence of technological parameters about cross rolling hollow part rolling work piece wall thickness change, *J. Agric Mach*, 27 (1) (1996) 108.

[4] X. D. Shu, *The Theory and Application on Multi-wedge Synchronous Cross Wedge Rolling*, Beijing: Science Press (2011) 2.

[5] X. D. Shu, C. M. Li and Z. H. Hu, Theoretical and experimental study of varying rule of rolling-moment about cross-wedge rolling, *Materials Processing Technology* (2007) 187-188, 752-756.

[6] X. D. Shu, The research on the process parameters impact on the forming mechanism multi-wedge cross wedge rolling, *Journal of University of Science and Technology Beijing*, 7 (2) (2005) 222-226.

[7] J. Zhao and X. D. Shu, Influence rules of technological parameters on interface quality of multi-wedge cross wedge rolling work piece, *Chinese Journal of Mechanical Engineering*, 44 (11) (2008) 209-214.

[8] J. Zhao, X. D. Shu and Z. H. Hu, Analysis of influence factors on mechanical parameters in multi-wedge cross rolling wedge forming automobile semi-axes, *Journal of University of Science and Technology Beijing*, 29 (1) (2007) 63-66.

[9] S. Urankar, M. Lovell and C. Morrow, Development of a critical friction model for cross wedge rolling hollow shafts, *Journal of Materials Processing Technology*, 177 (2006) 539-544.

[10] S. Urankar et al., Establishment of failure conditions for the cross wedge rolling of hollow shafts, *Journal of Materials Processing Technology*, 177 (2006) 545-549.

[11] Z. Pater, J. Kazaneckib and A. Gontarza, Study of the process stability of cross wedge rolling, *Journal of Materials Processing Technology* (1999) 458-462.

[12] J. Bartnicki and Z. Pater, The aspects of stability in cross-wedge rolling processes of hollowed shafts, *Journal of Materials Processing Technology* (2004) 155-156, 1867-1873.

[13] Z. Pater and J. Bartnicki, Finished cross wedge rolling of hollowed cutters, *Archives of Metallurgy and Materials*, 51 (2) (2006) 205.

[14] W. Ding, K. Zhang, C. Yang and Z. Hu, Study on the ovality of hollow shafts with equal inner diameter formed by

cross wedge rolling, *Journal of Plasticity Engineering*, 17 (3) (2010) 27-31.

[15] H. Ding, C. P. Yang and K. S. Zhang, Thermo mechanical coupled numerical simulation on cross wedge rolling of hollow shaft parts with equal inner diameters, *Journal of University of Science and Technology Beijing*, 32 (4) (2010) 25-529.

[16] H. C. Ji, *Research on Cross Wedge Rolling Forming and Microstructure Evolution of 21-4N for Hollow Valve*, University of Science and Technology Beijing (2017).

[17] C. P. Yang and Z. H. Hu, Influence of the flattening deformation on the forming of hollow parts in cross wedge rolling, *Journal of Beijing Institute of Technology*, 34 (9) (2014) 881-885.

[18] W. Peng et al., Multi-wedge cross wedge rolling process of 42CrMo4 large and long hollow shaft, *Rare Metal Materials & Engineering*, 45 (4) (2016) 836-842.

[19] P. H. Yu, X. D. Shu and W. F. Peng, Influence of process parameters on grain size of hollow shafts in multi-wedge cross wedge rolling, *Hot Working Technology*, 43 (1) (2014) 96-99.

[20] X. D. Shu, C. Liu and B. S. Sun, Influence of mold technological parameters on the forming force parameters in multi-wedge rolling of the railway hollow shafts, *Journal of Plastic Engineering*, 23 (3) (2016) 23-28.

Xuedao Shu is a Professor in Ningbo University, People's Republic of China. His major is Plastic Processing Technology and Equipment.